

Rossby Number Effects on Columnar Eddy Formation and the Energy Dissipation Law in Homogeneous Rotating Turbulence

T. Pestana¹† and S. Hickel¹

¹Department for Aerodynamics, Faculty of Aerospace Engineering, Kluyverweg 2, 2629 HS Delft, The Netherlands

(Received xx; revised xx; accepted xx)

Two aspects of homogeneous rotating turbulence are quantified through forced Direct Numerical Simulations in an elongated domain, which is in the direction of rotation about 340 times larger than the typical initial eddy size. First, by following the time evolution of the integral length-scale along the axis of rotation ℓ_{\parallel} , the growth rate of the columnar eddies and its dependency on the Rossby number Ro_{ε} is determined as $\gamma = 4 \exp(-17Ro_{\varepsilon})$, where γ is the non-dimensional growth rate. Second, a scaling law for the energy dissipation rate ε_{ν} is sought. Comparison with current available scaling laws shows that the relation proposed by Baqui & Davidson (2015), i.e., $\varepsilon_{\nu} \sim u'^3/\ell_{\parallel}$, where u' is the r.m.s. velocity, approximates well part of our data, more specifically the range $0.39 \leq Ro_{\varepsilon} \leq 1.54$. However, relations proposed in the literature fail to model the data for the second and most interesting range, i.e., $0.06 \leq Ro_{\varepsilon} \leq 0.31$, which is marked by the formation of columnar eddies. To find a similarity relation for the latter, we exploit the concept of a spectral transfer time introduced by Kraichnan (1965). Within this framework, the energy dissipation rate is considered to depend on both the non-linear time-scale and the relaxation time-scale. Thus, by analyzing our data, expressions for these different time-scales are obtained that results in $\varepsilon_{\nu} \sim u'^4/(\ell_{\perp}^2 Ro_{\varepsilon}^{0.62} \tau_{nl}^{iso})$, where ℓ_{\perp} is the integral length-scale in the direction normal to the axis of rotation and τ_{nl}^{iso} is the non-linear time-scale of the initial homogeneous isotropic field.

1. Introduction

Many geophysical and man-made fluid flows are affected by the interaction between system rotation and turbulence (Greenspan 1968; Boffetta & Ecke 2012). Still, our knowledge of the effects of the Coriolis force on turbulence is far from complete. An idealized approach to study rotating turbulence consists in observing the evolution of an initial homogeneous isotropic flow in a non-inertial rotating frame of reference. This way, early experimental studies already revealed the main features of homogeneous rotating turbulence, although a few of them did not meet the condition for homogeneity (Ibbetson & Tritton 1975; Hopfinger *et al.* 1982; Jacquin *et al.* 1990). When the Rossby number (Ro) was sufficiently small, i.e., the ratio of the rotational time scale and the turbulent time scale, it was observed that the energy dissipation rate ε_{ν} reduced with respect to the reference non-rotating isotropic case. Further, the typical cloud of isotropic eddies found in isotropic flows was strained, and grew in size to towards an array of flow structures aligned with the axis of rotation (columnar eddies). These two features are the traits of rotating turbulence and have been observed and analyzed in a number of

† Email address for correspondence: t.pestana@tudelft.nl

recent experimental and numerical investigations, see, e.g., Staplehurst *et al.* (2008); van Bokhoven *et al.* (2009); Mininni *et al.* (2009); Moisy *et al.* (2011); Delache *et al.* (2014); Mininni *et al.* (2012), or Godeferd *et al.* (2015) for a review. Yet, it remains poorly understood how they are quantitatively related.

For homogeneous isotropic turbulence, it is well accepted that the energy dissipation rate scales as $\varepsilon_\nu \sim u_0^3/l_0$, where u_0 and l_0 are an integral velocity scale and an integral length scale, respectively (Batchelor & Press 1953). This relation can be interpreted on the basis of phenomenological arguments as follows. Let us first assume that ε_ν depends on a energy content, say u_0^2 , and on a time scale τ_s characteristic of the downscale energy transfer: the spectral transfer time. In homogeneous isotropic turbulence, the only time scale available to be taken as τ_s is the time scale characteristic of the non-linear triadic interactions, τ_{nl} . If we further assume that $\tau_{nl} \sim l_0/u_0$, where l_0 is the typical size of the energy containing eddies, the dissipation law for homogeneous isotropic turbulence can be recovered. But for systems in which other time scales are also relevant, as is the case of magnetohydrodynamics (MHD) or rotating turbulence, τ_s might be different from τ_{nl} . Within the context of MHD, Kraichnan (1965) considered that τ_s is in fact composed of two time scales of opposing effects; the non-linear time scale τ_{nl} , which can also be considered as the measure of how fast triple velocity correlations are built-up, and the decorrelation time scale τ_3 , which indicates how fast these correlations decay in time. Exploiting these ideas, he suggested that the energy flux (energy dissipation rate) was directly proportional to τ_3 and inversely proportional to τ_{nl} .

Following this line of thought, one alternative to relate the energy dissipation rate to the formation of columnar eddies in rotating turbulence is to find approximations for τ_{nl} and τ_3 that involve integral length scales and the rotation rate. However, this is not straightforward. First, owing to the fact that the distribution of energy is not isotropic, two distinct integral length scales in homogeneous rotating turbulence exist, i.e., $\ell_{0\perp}$ and $\ell_{0\parallel}$, which can be defined along the directions normal and parallel to the axis of rotation, respectively. Which one then is relevant to form τ_{nl} ? Second, how does τ_3 depend on the time scale imposed by the background rotation, i.e., $\tau_\Omega = 1/(2\Omega)$? In literature, a few dissipation laws for homogeneous rotating turbulence have emerged from attempts to estimate the energy flux (Zhou 1995; Galtier 2003; Nazarenko & Schekochihin 2011; Baqui & Davidson 2015). Despite the efforts to account for the effects of rotation, results available in current literature regarding whether these laws generally hold or if they specifically apply to a Rossby number range are inconclusive or even inconsistent.

Another problem, which is rather more technical, is the fact that the elongated columnar flow structures restrict the maximum observation time in Direct Numerical Simulations (DNS) of rotating turbulence. Because simulations of homogeneous flows often consider periodic boundary conditions, a too small domain size with respect to the characteristic size of the living eddies can modulate the dynamics of the large scales and constrain their size. An obvious solution to circumvent this problem and avoid numerical artifacts is either to consider larger domains or to generate flow fields in which the characteristic eddy size is smaller than the domain size. For example, in the DNS by Baqui & Davidson (2015) the initial characteristic eddy size was 50 times smaller than the domain size. However, when $Ro \ll 1$ this may be still insufficient and limit the simulation to a few eddy-turnover times.

In view of these shortcomings, this study addresses the two following questions:

- (i) What is the influence of the Rossby number in the growth rate of the columnar eddies, in the absence of confinement effects?

- (ii) Can we approximate the energy dissipation rate in homogeneous rotating turbulence in a fashion similar to homogeneous isotropic turbulence, i.e., in terms of a velocity scale, an integral length scale and the rotation rate?

For this purpose, we consider the evolution of an initial homogeneous isotropic flow field in a rotating frame of reference. We conduct a systematic study that consists of 21 different rotation rates, thus covering a wide range of Rossby numbers. Our DNS are carried out in an elongated computational domain that is about 340 times larger than the initial characteristic size of the flow structures, provides enough room for the columnar eddies to grow freely. All simulations are performed with a stochastic large-scale forcing that injects energy at a constant rate. The forcing scheme is three-dimensional, isotropic, and at all times uncorrelated with the velocity field. To the best of our knowledge, the present database is unprecedented.

This work is organized as follows. In section 2, the governing equations and the numerical method is detailed together with a description of the simulations and their physical parameters. The influence of the Rossby number in the growth rate of the columnar eddies is investigated in section 3, and approximations for the energy dissipation rate are finally offered in section 4.

2. Numerical Set-up

2.1. Governing Equations and Numerical Method

We consider an incompressible fluid in a triply periodic rectangular cuboid of size $2\pi\mathcal{L}_1 \times 2\pi\mathcal{L}_2 \times 2\pi\mathcal{L}_3$ that rotates around $\boldsymbol{\Omega}$. Fluid motion is assumed governed by the incompressible Navier-Stokes equations:

$$\nabla \cdot \mathbf{u} = 0, \quad (2.1)$$

$$\frac{\partial \mathbf{u}}{\partial t} + (2\boldsymbol{\Omega} + \boldsymbol{\omega}) \times \mathbf{u} = -\nabla q + \nu \nabla^2 \mathbf{u} + \mathbf{f}. \quad (2.2)$$

Here, \mathbf{u} , $\boldsymbol{\omega}$ and \mathbf{f} are the velocity, the vorticity and an external force, respectively. Time is denoted by t , the reduced pressure, into which the centrifugal force is incorporated, is given by q , and ν denotes the kinematic viscosity of the fluid. The rotation vector $\boldsymbol{\Omega}$ is chosen to be aligned with the 3-direction, i.e. $\boldsymbol{\Omega} = (0, 0, \Omega)$, where Ω is the rotation rate. The horizontal dimensions of the rectangular cuboid (normal to the axis of rotation) are equal, $\mathcal{L}_\perp = \mathcal{L}_1 = \mathcal{L}_2 = 1$, whereas the vertical extension (parallel to the axis of rotation) is by a factor of 8 larger than the horizontal dimensions, i.e. $\mathcal{L}_\parallel = \mathcal{L}_3 = 8$.

The numerical method is essentially the same as in Pestana & Hickel (2019). Equations (2.1) and (2.2) are solved by a de-aliased Fourier pseudo-spectral method (2/3-rule), where the spatial gradients are computed with the aid of fast Fourier transforms (Pekurovsky 2012), and the time-stepper employs exact integration of the viscous and Coriolis forces (Rogallo 1977; Morinishi *et al.* 2001) together with a third-order low-storage Runge-Kutta scheme for the non-linear terms. The number of degrees of freedom is $N_p = 768^2 \times 6144$, which has been increased accordingly to the extended domain size to resolve all scales of motion. The smallest and largest resolved wavenumber per direction is $\kappa_{min,i} = 1/\mathcal{L}_i$ and $\kappa_{max,i} = N_{p,i}/(3\mathcal{L}_i)$, respectively, where the index $i = \{1, 2, 3\}$ denotes the different directions.

In all simulations considered in this study, energy is injected through the external force \mathbf{f} on right-hand-side of equation (2.2). The forcing scheme is designed as proposed in Alvelius (1999); the force spectrum $F(\kappa)$ is Gaussian with standard deviation $c = 0.5$

$\kappa_f \mathcal{L}_\perp$	$\kappa_f \mathcal{L}_\parallel$	$(2\pi \mathcal{L}_\perp)/\ell_\perp^{\text{iso}}$	$(2\pi \mathcal{L}_\parallel)/\ell_\parallel^{\text{iso}}$	τ_f/T_e	Re_ε	Re_λ	N_p
8	64	39.9	342.5	2.36	55.05	68	$768^2 \times 6144$

Table 1: Numerical and physical parameters of the initial homogeneous isotropic turbulent flow field used for the runs with rotation.

and is centered around the forcing wavenumber κ_f :

$$F(\kappa) = A \exp(-(\kappa - \kappa_f)^2/c). \quad (2.3)$$

In equation (2.3), the prefactor A , which controls the amplitude of $F(\kappa)$ can be determined *a priori* to the simulation and allow us to fix the power input ε_I . This is only possible because this forcing scheme ensures that the force-velocity correlation is at all time instants zero. As a consequence, the injected power is an exclusive product of the force-force correlation, which is directly related to $F(\kappa)$ (Alvelius 1999).

2.2. Description of the Simulations and Physical Parameters

To describe the considered physical problem, we are free to choose 6 control parameters. These form the set $\{\kappa_f, \varepsilon_I, \nu, \mathcal{L}_\parallel, \mathcal{L}_\perp, \Omega\}$, which involves two physical units. Thus, a total of 4 non-dimensional numbers is sufficient to describe the numerical experiment. The governing non-dimensional numbers can be built by combination of the free control parameters. For instance, using κ_f and ε_I and assuming that the constant of proportionality is 1, we can construct the velocity scale $u_f = \varepsilon_I^{1/3} \kappa_f^{-1/3}$ and the time scale $\tau_f = \kappa_f^{-2/3} \varepsilon_I^{-1/3}$. Additionally, a characteristic length scale can be taken as $\ell_f = 1/\kappa_f$. Hence, the Reynolds and the Rossby number are defined as

$$Re_\varepsilon = \frac{\varepsilon_I^{1/3} \kappa_f^{-4/3}}{\nu} \quad \text{and} \quad Ro_\varepsilon = \frac{\kappa_f^{2/3} \varepsilon_I^{1/3}}{2\Omega}. \quad (2.4)$$

The two other governing non-dimensional numbers are formed by combining the forcing wavenumber with the geometric dimensions of the domain to yield $\kappa_f \mathcal{L}_\perp$ and $\kappa_f \mathcal{L}_\parallel$. The 4 non-dimensional numbers, $\{Re_\varepsilon, Ro_\varepsilon, \kappa_f \mathcal{L}_\parallel, \kappa_f \mathcal{L}_\perp\}$, whose definitions have been borrowed from Seshasayanan & Alexakis (2018), form the parameter space henceforth used to characterize the simulations performed in this study. Note, however, that this set of non-dimensional parameters is not unique. For instance, one may combine Re_ε and Ro_ε to form the micro-scale Rossby number $Ro_\lambda = Re_\varepsilon^{1/2} Ro_\varepsilon$, which represents the ratio of rotation and Kolmogorov time scales, or express the geometric dimensions in terms of the domain aspect ratio $A_r = \mathcal{L}_\parallel/\mathcal{L}_\perp$.

Another important parameter is the Zeman wavenumber $\kappa_\Omega = (\Omega^3/\varepsilon_I)^{1/2}$, which indicates the wavenumber range for which rotational effects are relevant (Zeman 1994; Delache *et al.* 2014). The Zeman wavenumber is also automatically set by fixing the aforementioned parameters as $Ro_\varepsilon = (\kappa_f/\kappa_\Omega)^{2/3}/2$.

A posteriori, we can compute the usual physical parameters that describe the flow field. The box-averaged kinetic energy K is given by $\langle u_i u_i \rangle_{\mathcal{L}}/2$, where the operator $\langle \cdot \rangle_{\mathcal{L}}$ denotes volume averages, and the viscous dissipation rate is $\varepsilon_\nu = 2\nu \langle S_{ij} S_{ij} \rangle_{\mathcal{L}}$, where $S_{ij} = (\partial u_{i,j} + \partial u_{j,i})/2$ is the strain-rate tensor. From K , we define the r.m.s. velocity $u' = \sqrt{2K/3}$, which is used to define the large-eddy turnover time $T_e = u'^2/\varepsilon_I$. The Taylor micro-scale is defined as in Pope (2000), i.e., $\lambda = (15\nu u'^2/\varepsilon_\nu)^{1/2}$. The Taylor

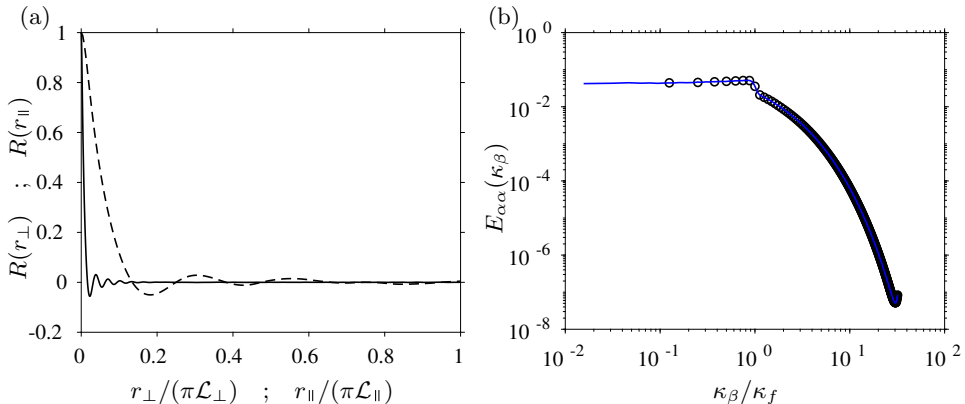


Figure 1: Two-point velocity correlations showing the ratio domain size to characteristic size of the flow structures in the different directions, and one-dimensional energy spectra showing that the initial conditions are indeed isotropic. (a) Normal $R(r_{\perp})$ (- - -) and parallel $R(r_{\parallel})$ (—) velocity two-point correlations. (b) Perpendicular and parallel one-dimensional energy spectra: $\alpha = 1$; $\beta = 3$; $E_{11}(\kappa_3)$ (—) and $\alpha = 3$; $\beta = 1$; $E_{33}(\kappa_1)$ (\circ)

micro-scale Reynolds number is computed as $Re_{\lambda} = u'\lambda/\nu$, and the Kolmogorov length scale is $\eta = (\nu^3/\varepsilon_I)^{1/4}$.

Last, we define the integral length scales along the directions normal and parallel to the axis of rotation. These are constructed from the two-point velocity correlation:

$$R(\mathbf{r}) = \frac{\langle u_i(\mathbf{x})u_i(\mathbf{x} + \mathbf{r}) \rangle_{\mathcal{L}}}{\langle u_i(\mathbf{x})u_i(\mathbf{x}) \rangle_{\mathcal{L}}}, \quad (2.5)$$

where $\mathbf{r} = r_i\hat{\mathbf{e}}_i$ is an arbitrary position vector. We integrate equation (2.5) with $\mathbf{r} = r\hat{\mathbf{e}}_r$, as in spherical coordinates, or with $\mathbf{r} = r_{\perp}\hat{\mathbf{e}}_{\perp}$ and $\mathbf{r} = r_{\parallel}\hat{\mathbf{e}}_{\parallel}$, as in cylindrical coordinates, to obtain the integral length scales along the respective directions:

$$\ell = \int_0^{\pi\mathcal{L}_{min}} R(r) dr, \quad \ell_{\perp} = \int_0^{\pi\mathcal{L}_{\perp}} R(r_{\perp}) dr_{\perp}, \quad \text{and} \quad \ell_{\parallel} = \int_0^{\pi\mathcal{L}_{\parallel}} R(r_{\parallel}) dr_{\parallel}. \quad (2.6)$$

In equation (2.6), \mathcal{L}_{min} is taken as $\min(\mathcal{L}_{\parallel}, \mathcal{L}_{\perp})$ in the limit of the integral that defines ℓ . To represent quantities from the initial and isotropic flow field we use the superscript “iso”, like in ℓ^{iso} .

The initial conditions for the simulations with rotation are produced by injecting energy at constant rate ε_I to a fluid that is initially at rest. The energy, which is injected at wavenumber $\kappa_f = 8$, is progressively distributed over a wider range of wavenumbers by action of the triple velocity correlations. When the energy cascade is built-up, the box-averaged kinetic energy K stops growing and a steady-state is reached. The numerical resolution guarantees that at all times $\kappa_{max}\eta \geq 1.5$, which is sufficient to resolve all scales of motion. The initial transient lasts for $20\tau_f$ or, equivalently, $8.45T_e$, and afterwards, statistics are collected for another $54\tau_f$ ($22.84T_e$). For the fully developed field, we find that $Re_{\lambda} \approx 68$, and that the relation $\ell^{iso} = \ell_{\parallel}^{iso} = \ell_{\perp}^{iso}$ holds up to 2 decimal places. The latter suggests that the flow field is in fact isotropic.

Other statistics of the steady-state match closely with typical values found in DNS of homogeneous isotropic turbulence. For instance, the skewness and flatness of the longitudinal velocity derivative $\partial u_1/\partial x_1$ are -0.51 and 4.8 , respectively, in agreement with Tang *et al.* (2018) and Van Atta & Antonia (1980). The energy dissipation rate ε_{ν}

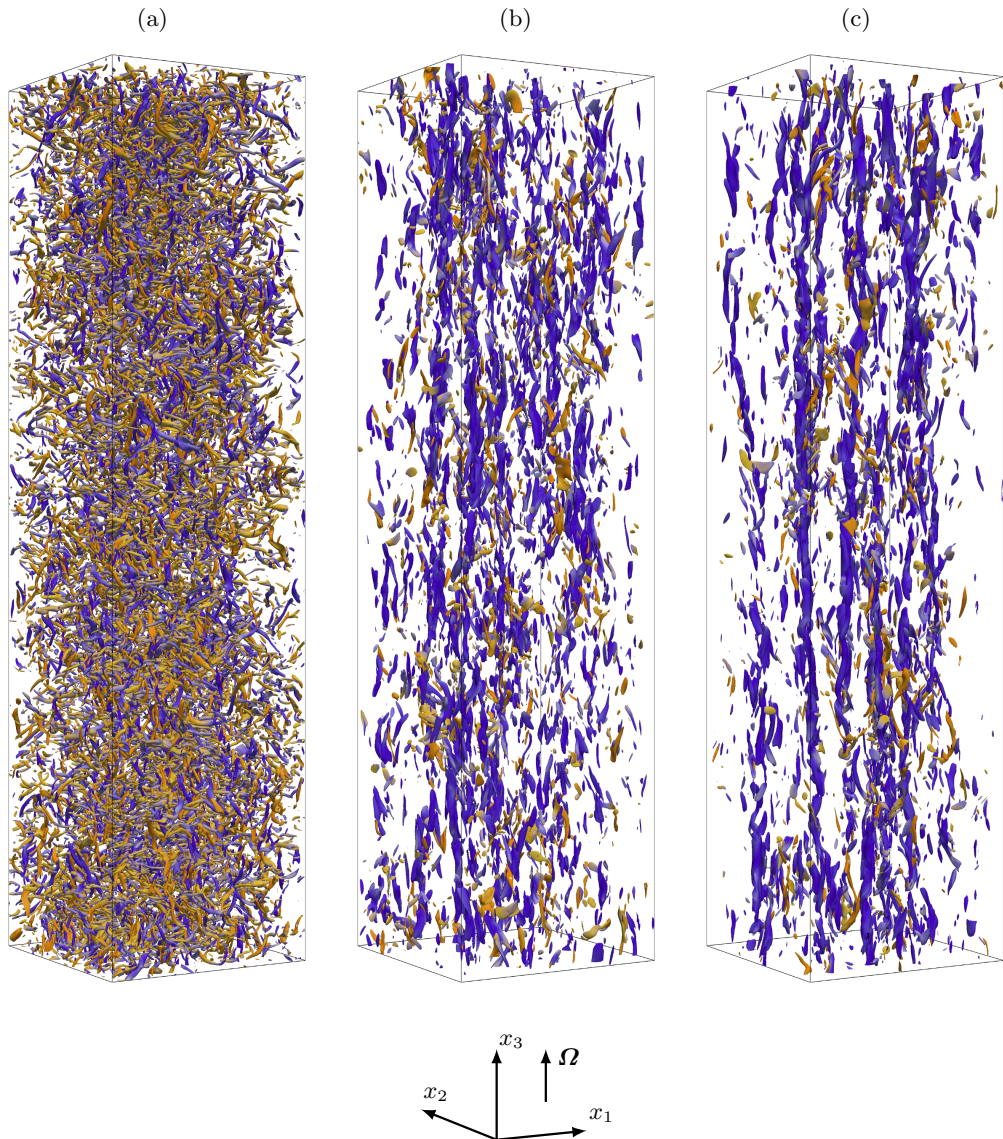


Figure 2: Flow field visualization of a sub-set of the computational domain ($1/16$ of the entire computational domain), showing half of the horizontal domain extension and $1/4$ of the vertical domain size: $[0, \pi] \times [0, \pi] \times [0, 4\pi]$. Iso-contours of the Q-criterion (Hunt *et al.* 1988) colored by the normalized projection of the vorticity vector along the axis of rotation, i.e., $\boldsymbol{\omega} \cdot \mathbf{e}_\parallel / \|\boldsymbol{\omega}\|$. Blue colors indicates structures that rotate in the same sense as $\boldsymbol{\Omega}$ (counter-clockwise), whereas orange colors indicate the opposite sense of rotation (clockwise). (a) Isotropic initial condition; (b) and (c) correspond to the run with $Ro_\varepsilon = 0.06$ at later time instants after the onset of rotation, i.e., $t = 10.5 \tau_f$ and $t = 20 \tau_f$, respectively.






















	Run	Colormap	Ro_ε	Ro_λ	$\kappa_\Omega\eta$	κ_Ω/κ_f
R1	run01		1.54	11.42	0.009	0.19
	run02		1.25	9.28	0.013	0.25
	run03		1.00	7.42	0.017	0.35
	run04		0.87	6.45	0.022	0.44
	run05		0.77	5.71	0.026	0.52
	run06		0.69	5.12	0.031	0.62
	run07		0.63	4.64	0.035	0.72
	run08		0.56	4.12	0.042	0.85
	run09		0.47	3.45	0.055	1.11
	run10		0.39	2.91	0.071	1.44
R2	run11		0.31	2.32	0.100	2.02
	run12		0.27	2.01	0.124	2.52
	run13		0.24	1.79	0.148	2.99
	run14		0.22	1.60	0.175	3.55
	run15		0.19	1.40	0.213	4.31
	run16		0.16	1.20	0.270	5.46
	run17		0.14	1.00	0.352	7.12
	run18		0.11	0.80	0.492	9.95
	run19		0.09	0.70	0.599	12.12
	run20		0.08	0.60	0.759	15.34
	run21		0.06	0.47	1.088	21.99

Table 2: Numerical and physical parameters for the DNS of homogeneous rotation turbulence at distinct rates of rotation. The runs that exhibit similar dynamics are collected together in groups, namely $R1$ and $R2$.

at the steady-state is well approximated by $\varepsilon_\nu = C_\varepsilon^{\text{iso}}(u'^{\text{iso}})^3/\ell^{\text{iso}}$, where $C_\varepsilon^{\text{iso}} \approx 0.35$ is the constant of proportionality. Note, however, that the value of this constant depends on how the two-point correlation in equation (2.5) is normalized. If we normalize it with $2u'$, like in Kaneda *et al.* (2003), instead of $2K$, like in equation (2.5), a factor of $3/2$ must be accounted for to yield $C_\varepsilon^{\text{iso}} \approx 0.5$ in agreement with literature; see Ishihara *et al.* (2009) for a compilation of other numerical results.

In this study, the goal is not to achieve the highest possible Reynolds number for a given numerical resolution. Instead, we focus on maximizing the time for which large scale eddies with typical size ℓ^{iso} can evolve unbounded, while still resolving all scales of motion. Therefore, apart from forcing at scales smaller than usual, we consider an elongated domain with $A_r = 8$. As a result, the isotropic fields to which background rotation can be imposed to are in the vertical direction about 340 times larger than ℓ^{iso} and, in the normal direction, $2\pi\mathcal{L}_\perp/\ell^{\text{iso}} \approx 40$. In figure 1, we show evidence of these aspects. Figure 1a confirms through the two-point velocity correlation along the normal and the parallel directions that the ratio domain size to flow structures is indeed significantly larger in the vertical direction. Alongside, figure 1b verifies that the velocity fields are isotropic, as the curves for the one-dimensional energy spectra along the normal and perpendicular directions overlap.

These features are also clearly visible in the flow field visualization; see figure 2, where we show a sub-set of the computational domain with the flow structures visualized by the Q-Criterion of Hunt *et al.* (1988) and colored by the normalized projection of the vorticity vector on the axis of rotation, i.e., $\boldsymbol{\omega} \cdot \mathbf{e}_\parallel / \|\boldsymbol{\omega}\|$. Reinforcing the aforementioned results, we observe two main points in the isotropic field that is used as initial condition for the runs

with rotation (figure 2a). First, the flow structures do not display any preferential sense of rotation, which is confirmed by the uniform distribution of the colors. Second, they are also isotropically arranged and therefore not aligned along any preferential direction. For a summary of the numerical and physical parameters of the initial conditions, please refer to table 1.

The runs with rotation are constructed by imposing 21 different background rotation rates to the isotropic flow field shown in figure 2a; see table 2 for the relevant numerical and physical parameters. The result is a set of simulations that covers a broad range of the Ro_ε parameter space, i.e., $0.06 > Ro_\varepsilon > 1.54$. The Zeman wavenumber in terms of the Kolmogorov length scale, $\kappa_{\Omega}\eta$, for instance, varies from 0.1 for $Ro_\varepsilon = 1.54$ (weakest rotation case) to 1.1 for $Ro_\varepsilon = 0.06$ (strongest rotation case). As the numerical resolution provides $\kappa_{max}\eta = 1.5$ for the fully developed isotropic reference initial field, for $Ro_\varepsilon = 0.06$, almost all scales of motion are influenced by the system's rotation.

The effects of rotation on the flow structures are readily seen in the flow-field visualization in figure 2. Together with the initial conditions, we see in figures 2b and 2c two snapshots for the run with $Ro_\varepsilon = 0.06$ at times subsequent to the onset of rotation ($t = 10.5\tau_f$ and $t = 20\tau_f$). In agreement with common knowledge, we confirm that the rotation destroys the small structures and modulates the flow field such that columns elongated in the direction of rotation emerge. At the later instant of time (figure 2c), structures in blue predominate, indicating that flow structures that rotate in the same sense as the imposed background rotation are more likely to be found. This is commonly referred to as the cyclone asymmetry and has been observed in the experiments of van Bokhoven *et al.* (2009) and in the computations of Bartello *et al.* (1994).

3. The Growth Rate of Columnar Eddies

Now, we present results and discuss the influence of different rotation rates on the growth of the columnar eddies. For the quantitative analysis, we use integral length scales, which on one hand can be used to quantify the typical eddy size that contributes the most to the total kinetic energy, and on the other hand also serves as an indicator of anisotropy. Due to the background rotation, the dynamics of the flow in the parallel and transversal direction are essentially different, which is reflected in the temporal evolution of ℓ_{\parallel} and ℓ_{\perp} (Bardina *et al.* 1985). As it will be seen, the appearance of the columnar eddies in figures 2b and 2c is strongly reflected in the growth of the integral length scale along the axis of rotation.

We obtain the time evolution of ℓ_{\parallel} and ℓ_{\perp} by evaluating equation (2.6) on a series of instantaneous velocity fields throughout the simulation time, see figure 3. We choose to split the actual data in two diagrams, which are displayed side-by-side. The left panels correspond to cases for which $Ro_\varepsilon \geq 0.39$ (group R1 in table 2) and the right panels to $Ro_\varepsilon \leq 0.31$ (group R2 in table 2). We organized the results in this manner, so cases with similar dynamics are shown together.

For $Ro_\varepsilon \geq 0.39$ (left panels; group R1), ℓ_{\parallel} and ℓ_{\perp} remain approximately unchanged in time and at values similar to the ones at $t = 0$, which corresponds to the initial isotropic field. Specifically for $Ro_\varepsilon = 0.39$, the run with highest rotation rate in this group, the departure from isotropy is marginal and $\ell_{\parallel}/\ell_{\perp} \approx 1.5$ at the final simulation time. Differently, for $Ro_\varepsilon \leq 0.31$ (right panels; group R2), the disparity between ℓ_{\parallel} and ℓ_{\perp} is clear. We observe that ℓ_{\parallel} grows substantially in time, whereas variations in ℓ_{\perp} are small when compared to the latter. For instance, for $Ro_\varepsilon = 0.06$, the final value of ℓ_{\parallel} is 26.8 times greater than its initial value, whereas ℓ_{\perp} only increases by a factor of 1.21. Additionally, we observe an intriguing behavior in ℓ_{\perp} . It initially grows in time until a

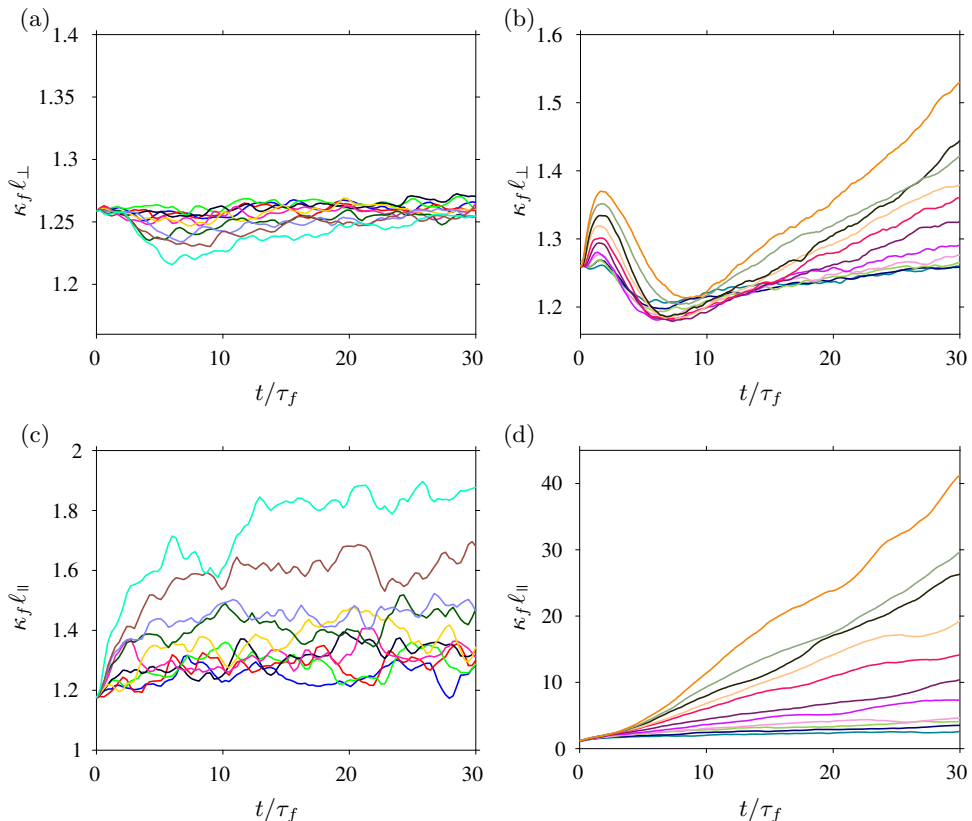


Figure 3: Time evolution of the parallel and transversal integral length scales ℓ_{\parallel} and ℓ_{\perp} , for $1.56 \geq Ro_{\varepsilon} \geq 0.39$ (left panels) and $0.31 \geq Ro_{\varepsilon} \geq 0.06$ (right panels)

maximum is reached; thereupon, it decreases towards a minimum, before growing again. On the other hand, ℓ_{\parallel} increases monotonically and approximately linearly for $t > 10\tau_f$.

The growth of ℓ_{\parallel} in figure 3d is in agreement with the formation of columnar eddies observed in figure 2c. In order to identify the dependency between the growth rate of ℓ_{\parallel} and Ro_{ε} , we have fit the data for ℓ_{\parallel} in the interval $10\tau_f < t < 30\tau_f$ with a straight line. The linear fit approximates fairly well the time evolution of ℓ_{\parallel} and the maximum residuum is found for $Ro_{\varepsilon} = 0.11$, where the discrepancy is around 4.7% of the mean value of ℓ_{\parallel} . The slope of the linear fit non-dimensionalized with the forcing parameters, i.e., $\gamma = \kappa_f \tau_f (d\ell_{\parallel}/dt)$, is shown in figure 4 as a function of Ro_{ε} . For $Ro_{\varepsilon} \geq 0.39$, the effects of rotation are irrelevant and γ approaches zero, suggesting that the integral length scales remain approximately at their initial value. On the other hand, the range $Ro_{\varepsilon} \leq 0.31$ is marked by a significant rise in γ . Overall, we find that the exponential dependency $\gamma = a \exp(b Ro_{\varepsilon})$ with $a = 4$ and $b = -17$ reproduces our data-set best.

Throughout this section, we have used integral length scales based on two-point velocity correlations to refer to vortex elongation. However, we must bear in mind the results obtained by Yoshimatsu *et al.* (2011), who showed that although a compact spherical vortex blob subjected to pure linear dynamics grows preferentially along the axis of rotation, ℓ_{\parallel} did not display any substantial growth. This conundrum was attributed to the fact that integral length scales based on the velocity field, such as ℓ_{\parallel} and ℓ_{\perp} , are fully determined by the amplitude of the diagonal elements of the velocity spectrum

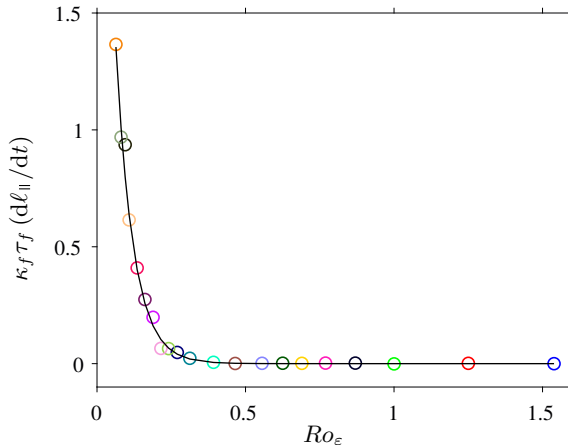


Figure 4: Growth rate of ℓ_{\parallel} in terms of Ro_{ε} , obtained after linear regression in the interval $10 \tau_f < t < 30 \tau_f$ of figures 3c and 3d. The residual of the linear fit is maximum for $Ro_{\varepsilon} = 0.11$ and around 4.7% of the mean value of ℓ_{\parallel} in the same interval. The blue solid line represents an exponential dependence on Ro_{ε} of the type $a \exp(b Ro_{\varepsilon})$, where $a = 4$ and $b = -17$ (—).

tensor. In other words, ℓ_{\parallel} and ℓ_{\perp} lack phase information. As alternative, it was then proposed to build integral length scales from nonlinear quantities, as these contain phase information. Instead, when integral length scales defined from the two-point correlation of the squared vorticity are used, the elongation of the initial compact eddy blob was successfully captured. We have verified that when non-linear dynamics are considered, i.e., when the Navier-Stokes equation (2.2) are used, both definitions of the integral length scale increase in time and evidence the elongation of vortices along the axis of rotation.

Further, note that to prevent the results from being affected by numerical artifacts, we stopped the simulations when ℓ_{\parallel} was about 8 times smaller than $2\pi\mathcal{L}_{\parallel}$. This constraint limited our runs to a duration of $30 \tau_f$ ($12.7 T_e$), and was due to the simulation with $Ro_{\varepsilon} = 0.06$. Obviously, for the remaining cases, $2\pi\mathcal{L}_{\parallel}/\ell_{\parallel} > 8$ at $t = 30 \tau_f$. The decision of when to interrupt the runs were rather arbitrary, but a value of 8 for the ratio $2\pi\mathcal{L}_{\parallel}/\ell_{\parallel}$ is common in DNS of homogeneous isotropic turbulence (Cardesa *et al.* 2017).

4. Scaling Laws for the Energy Dissipation Rate

The analysis for the integral length scales in the previous section has identified two regimes in our data-set. Whereas the group of runs *R1* display a dynamics similar to homogeneous isotropic turbulence, runs in the group *R2* are characterized by strong anisotropy. In this section, we present results for the evolution of the energy dissipation rate and seek for similarity relations that can collapse the data in the different regimes.

After the onset of rotation, both K and ε_{ν} evolve in time according to the conservation of energy, i.e., $dK/dt = -\varepsilon_{\nu} + \varepsilon_I$. While K grows rapidly (figure 5a), the viscous dissipation ε_{ν} first decreases monotonically until a minimum that is inversely proportional to Ro_{ε} is reached at roughly $t = 3 \tau_f$ (figure 5b). After reaching its lowest value, ε_{ν} continues to grow towards the power input ε_I , although the inequality $\varepsilon_{\nu} < \varepsilon_I$ remains for some of the cases up to the final simulation time. Generally speaking, the mismatch between the energy dissipation rate and the energy input rate in figure 5b is stronger for smaller Ro_{ε} (group *R2*).

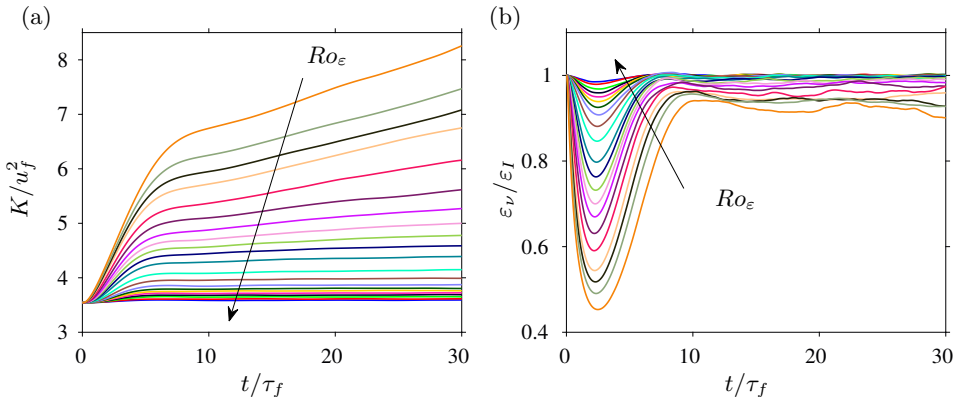


Figure 5: Time evolution of the box averaged kinetic energy K and energy dissipation rate ε_ν over time.

In fact, the imbalance $\varepsilon_\nu \neq \varepsilon_I$ is the footprint of an inverse energy cascade that is triggered by the Coriolis force, and that leads to the accumulation of energy at the large scales. This is expected to occur when Ro_ε is below a critical Rossby number that depends on the geometrical dimensions of the system (Smith *et al.* 1996; Deusebio *et al.* 2014; Pestana & Hickel 2019). In such cases, however, equilibrium ($\varepsilon_\nu = \varepsilon_I$) can still be restored after long integration times when the energy in the wavenumbers $\kappa < \kappa_f$ is sufficiently high to contribute to ε_ν (Valente & Dallas 2016; Seshasayanan & Alexakis 2018). For the runs considered in this study, the critical Ro_ε is approximately 1 as show in Pestana & Hickel (2019).

From figure 5b, it is evident that a naive scaling in terms of the forcing parameters can not cause the different lines in figure 5b to collapse, as it would in homogeneous isotropic turbulence. In other words, an approximation of ε_ν in terms of u_f and κ_f is invalid because the evolution of ε_ν in figure 5b depends clearly on Ro_ε . In homogeneous isotropic turbulence, the estimation $\varepsilon_\nu \sim u_f^3 \kappa_f$ suffices since both u_f and $1/\kappa_f$ are proportional to a characteristic velocity and a characteristic length, and this expression is equivalent to $\varepsilon_\nu \sim (u'^{\text{iso}})^3 / \ell^{\text{iso}}$. We must therefore search for other ways to approximate ε_ν in rotating turbulence.

4.1. Spectral Transfer Time

To address this problem we followed the methodology introduced by Kraichnan (1965) within the context of MHD and bridged by Zhou (1995) to homogeneous rotating flows. The basic idea is that the rate at which energy is transferred to the smaller scales depends on an energy content and on a time scale, viz. the spectral transfer time. If we treat the characteristic scales as global quantities instead of wavenumber dependent, the dissipation law can be written in terms of the r.m.s. velocity and the spectral transfer time as

$$\varepsilon_\nu \sim \frac{u'^2}{\tau_s}. \quad (4.1)$$

The spectral transfer time, however, is composed of two additional time scales, namely the nonlinear time scale τ_{nl} and the relaxation time scale τ_3 . Whereas τ_{nl} indicates how fast the triple velocity correlations are built up and favors the forward energy cascade, τ_3 serves as a relaxation time or a measure of how fast the triple velocity correlations are destroyed. The assumptions that the energy dissipation rate ε_ν is directly proportional

to τ_3 and that the energy cascade is local lead to the so-called “golden rule” (Zhou 1995):

$$\tau_s \sim \frac{\tau_{nl}^2}{\tau_3}. \quad (4.2)$$

In equation (4.2), τ_{nl} involves a velocity and a length scale and τ_3 can rest on any other time scales that are relevant for the problem. For instance, in forced homogeneous isotropic flows, $\tau_3 \sim \tau_f \sim \tau_{nl} \sim \ell^{\text{iso}}/u'^{\text{iso}}$, which implies $\tau_s \sim \ell^{\text{iso}}/u'^{\text{iso}}$ to recover the well known dissipation law $\varepsilon_\nu \sim (u'^{\text{iso}})^3/\ell^{\text{iso}}$, extensively verified by DNS and experiments. For more complex flows, which involve other time scales like rotating turbulence with the rotation time scale $\tau_\Omega = 1/(2\Omega)$, the relaxation time scale τ_3 can be assumed as function of the type $\tau_3 = \tau_3(\tau_f, \tau_\Omega)$ (Kraichnan 1965; Zhou 1995; Matthaeus & Zhou 1989). Combining equations (4.1) and (4.2) leads to

$$\varepsilon_\nu \sim u'^2 \left(\frac{\tau_3}{\tau_{nl}^2} \right), \quad (4.3)$$

and the problem of determining the dissipation law becomes the one of determining τ_{nl} and τ_3 .

4.2. Evaluation of Current Available Dissipation Laws

In current literature, a few dissipation laws for homogeneous rotating turbulence have been proposed. For example, the approximations that follow from the theory of Zhou (1995); Galtier (2003); Nazarenko & Schekochihin (2011) and Baqui & Davidson (2015) are

$$\varepsilon_\nu \sim \frac{u'^4}{\Omega \ell^2}, \quad \varepsilon_\nu \sim \frac{u'^4 \ell_\parallel}{\Omega \ell_\perp^3}, \quad \varepsilon_\nu \sim \frac{u'^3}{\ell_\perp}, \quad \text{and} \quad \varepsilon_\nu \sim \frac{u'^3}{\ell_\parallel}, \quad (4.4)$$

respectively. Although these authors do not explicitly present their theories within the framework of a spectral transfer time, we have taken the freedom to also summarize the theories within this context.

The law proposed by Zhou (1995), for instance, ignores anisotropy. It assumes that $\tau_{nl} \sim \ell/u'$ and that the relaxation time scale is proportional to the rotation time scale, i.e., $\tau_3 \sim \tau_\Omega$, to yield $\varepsilon_\nu \sim u'^4/(\Omega \ell^2)$. In contrast, dimensional analysis for the weak inertial-wave theory proposed by Galtier (2003), which takes into account scale anisotropy, results in $\varepsilon_\nu \sim u'^4 \ell_\parallel / (\Omega \ell_\perp^3)$, where $\tau_{nl} \sim \ell_\perp/u'$ and $\tau_3 \sim \ell_\parallel / (\Omega \ell_\perp)$. When anisotropy is however disregarded, i.e., $\ell \sim \ell_\parallel \sim \ell_\perp$, the predictions by Galtier (2003) reduce to the relation proposed by Zhou (1995). The critical balance theory of Nazarenko & Schekochihin (2011) considers that $\tau_{nl} \sim \tau_3 \sim \ell_\perp/u'$ and the theory of Baqui & Davidson (2015) suggests that $\tau_{nl} \sim \tau_3 \sim \ell_\parallel/u'$.

When we apply the scaling laws in equation (4.4) to the data presented in figure 5b, we observe overall a poor prediction; see figure 6. The approximations of Zhou (1995); Galtier (2003); Nazarenko & Schekochihin (2011) in figures 6a to 6c are found insufficient as the different curves are far away from collapsing into a single curve. For large Ro_ε , figure 6a delivers at least straight lines, suggesting a correction factor in terms of Ro_ε . For small Ro_ε , however, deviations from a straight line are evident. In figure 6b, the curves of the 5 last runs in group *R2* (lowest Ro_ε) seems to follow a similar trend, yet for high Ro_ε a poor match is again found. Differently, figure 6c shows that for large Ro_ε and $t > 10 \tau_f$, the curves are flat and tend closer to another. This is expected as ℓ_\perp must tend to ℓ^{iso} for large Ro_ε , and, in this limit, the dissipation law of homogeneous isotropic turbulence is recovered.

The best approximation, at least for part of the data-set, is obtained with the scaling

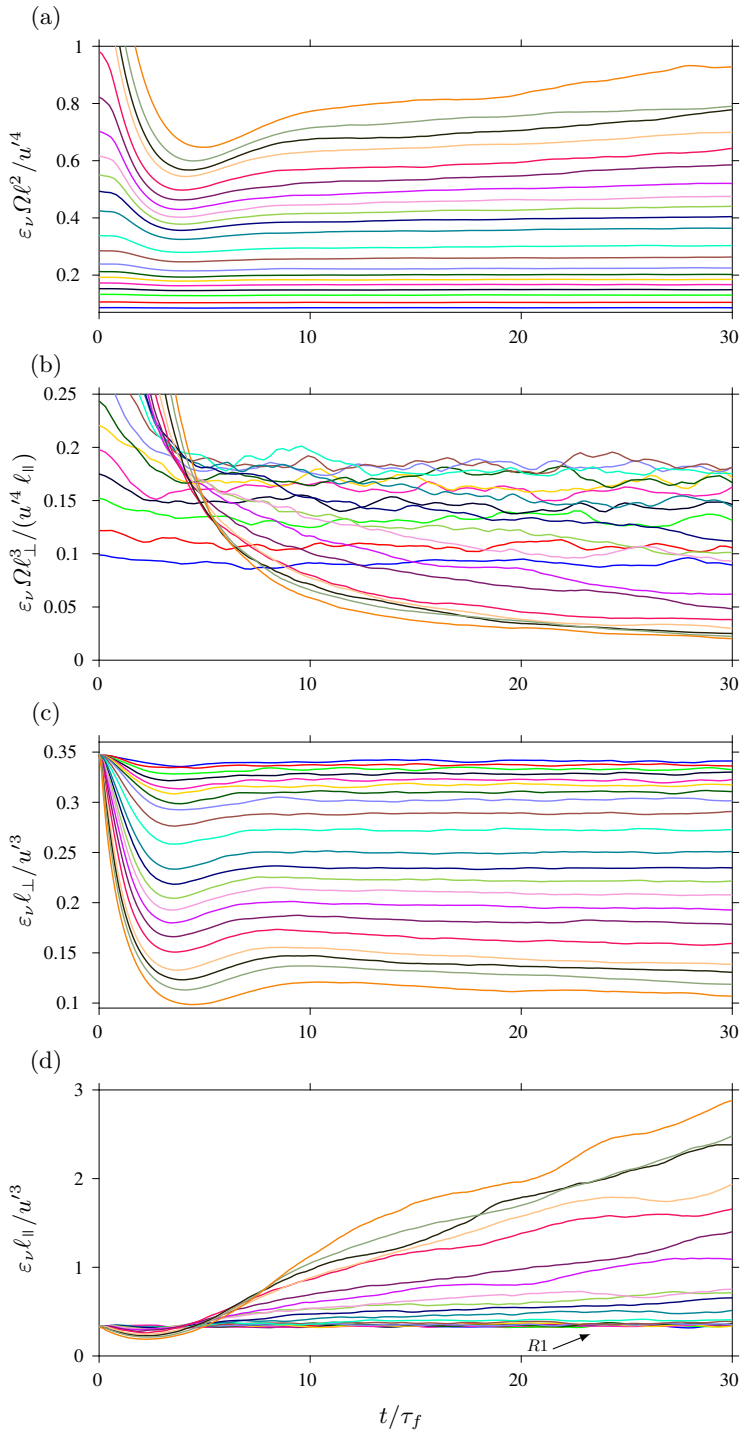


Figure 6: Compensated time evolution of the energy dissipation rate for $0.06 < Ro_\varepsilon < 1.54$. Different panels correspond to the different scaling laws found in the literature: (a) Zhou (1995); (b) Weak inertial-wave theory Galtier (2003); (c) Critical balance theory Nazarenko & Schekochihin (2011); (d) Baqui & Davidson (2015).

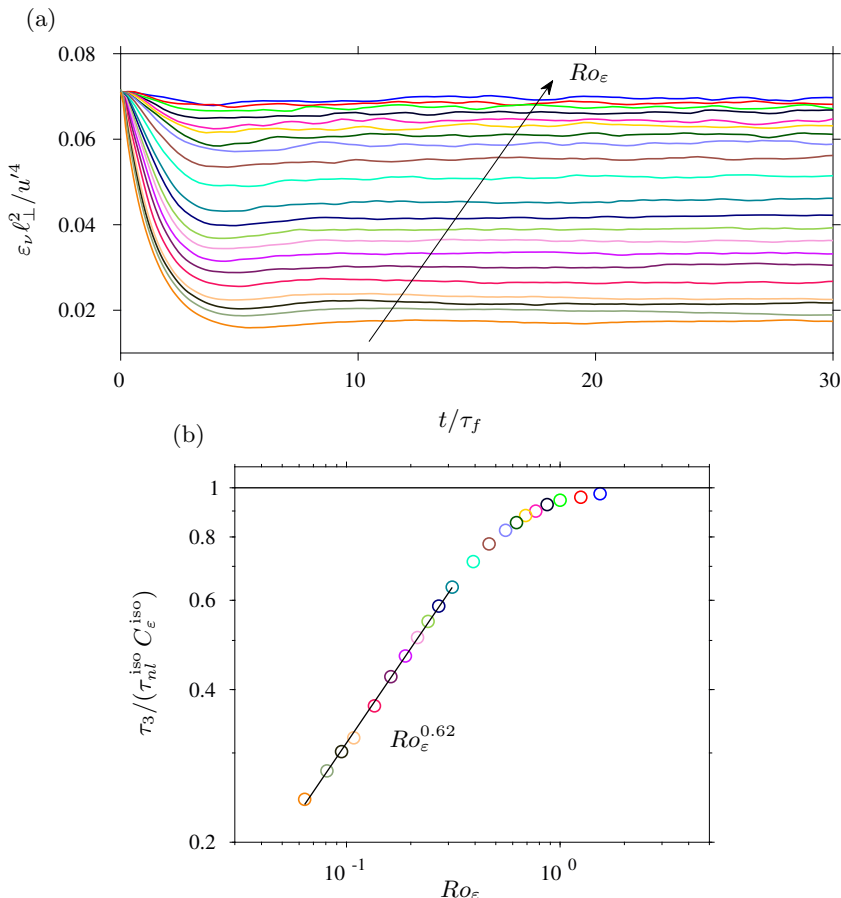


Figure 7: Decorrelation (relaxation) time scale τ_3 as function of time (a) and averaged over the interval $10 \leq t \leq 30 \tau_f$ and normalized by the the non-linear time scale τ_{nl} times the proportionality constant $C_\varepsilon^{\text{iso}}$ (b). Two reference lines are included. The horizontal line at the top signalizes that for large Ro_ε , the relaxation time scale tends to the value of the non-linear time scale of the homogeneous isotropic case. The other line shows the power-law dependency of the type Ro_ε^h with $h = 0.62$ for runs of the group *R2*.

law of Baqui & Davidson (2015). Figure 6d indicates that this scaling is suitable for the runs in group R1 (indicated with an arrow in the figure). For the other runs in group R2, figure 6d also provides unsatisfactory results like the other scaling laws. We are then motivated to look into a similarity law for this group of runs.

4.3. A Dissipation Scaling Law for Runs in Group R2

To find a dissipation law for runs in group R2 we base ourselves on equation (4.3). The first question we turn to is the one of finding an approximation for τ_{nl} . The non-linear time scale involves an estimation of a velocity and a length scale, which we shall assume as u' and ℓ_\perp , respectively. The reason behind this choice goes as follow. From figures 3d and 5b, we observe that ℓ_\perp and ε_ν display similar dynamics, although inverse; the evolution of each variable is the opposite of the other. This behavior hints to a dependency of the form $\varepsilon_\nu \sim 1/\ell_\perp$, which can also be justified like in the critical balance theory (Nazarenko & Schekochihin 2011). Within this theory, the basic idea is that

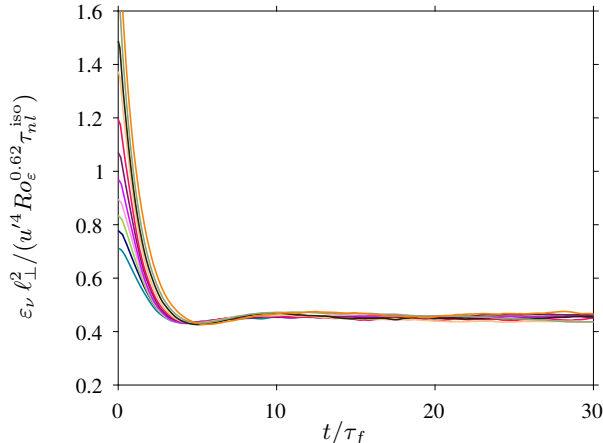


Figure 8: Time evolution of the energy dissipation rate scaled according to equation (4.6) for $Ro_\varepsilon \leq 0.31$.

rotation tends to destroy derivatives along the direction of rotation and the advection term is mainly due to the normal velocity gradients and the normal velocity field. Thus, ℓ_\perp is taken as the relevant length scale for the non-linear interactions. On the other hand, for the velocity scale, an alternative would be to take information about the transversal velocity fields only as in Baqui & Davidson (2015). Nevertheless, although rotation favors two dimensionalization, the velocity field remains three component and the anisotropy in the Reynolds stress tensor is minimal Yeung & Zhou (1998). For the above reasons, we assume $\tau_{nl} \sim \ell_\perp / u'$, and equation (4.3) can be in a preliminary step expressed as

$$\varepsilon_\nu \sim \frac{u'^4}{\ell_\perp^2} \tau_3(\tau_f, \tau_\Omega). \quad (4.5)$$

Now, to determine the relaxation time scale, we rearrange equation (4.5) so that τ_3 appears as a function of the other terms and examine its temporal evolution. Figure 7a shows $\tau_3 \sim \varepsilon_\nu \ell_\perp^2 / u'^4$ over time for all runs. After a transient of approximately $10 \tau_f$, we observe that the curves for different Ro_ε reach a plateau, with a terminal value that depends on Ro_ε . To determine this dependency, results from figure 7a are then averaged in the interval $10 \tau_f < t < 30 \tau_f$ and the mean value is shown against the corresponding Rossby number in figure 7b. In the latter figure, the ordinates appear normalized by the nonlinear time scale τ_{nl}^{iso} times $C_\varepsilon^{\text{iso}}$, which is the constant of proportionality of the dissipation law in homogeneous isotropic turbulence. For runs in group R1, $\tau_3 / (\tau_{nl}^{\text{iso}} C_\varepsilon^{\text{iso}})$ increases with Ro_ε and asymptotically approaches 1, implying that for these Ro_ε the effects of rotation are negligible and the scaling law of homogeneous isotropic turbulence is recovered. Contrarily and more surprising, we see that $\tau_3 / (\tau_{nl}^{\text{iso}} C_\varepsilon^{\text{iso}})$ follow the power-law Ro_ε^h with $h = 0.62$ for the runs in group R2. Consequently, for this group, we can finally express equation (4.5) as

$$\varepsilon_\nu \sim \frac{u'^4}{\ell_\perp^2} (\tau_{nl}^{\text{iso}} Ro_\varepsilon^{0.62}) \sim \frac{u'^3}{\ell_\perp} \left[\left(\frac{\tau_{nl}^{\text{iso}}}{\tau_{nl}} \right) Ro_\varepsilon^{0.62} \right]. \quad (4.6)$$

Equation (4.6) summarizes the effects of rotation for the runs with $0.06 < Ro_\varepsilon < 0.31$, and suggests that in a rotating frame of reference, the disparity between τ_{nl} and τ_{nl}^{iso} increases, such that the ratio $(\tau_{nl} / \tau_{nl}^{\text{iso}})$ shrinks with the inverse of $Ro_\varepsilon^{0.62}$. Finally, scaling

the data in figure 5b with equation (4.6) leads to figure 8, where very good agreement is found for all the cases in group *R2*.

5. Conclusions

We have investigated the effects of system rotation with Rossby numbers in the range $0.06 \leq Ro_\varepsilon \leq 1.54$ on the evolution of an initial cloud of isotropic eddies. Differently from other studies, which have focused on the initial transient immediately after the onset of rotation, we have focused instead on longer time intervals. This was only possible because our DNS were carried out in elongated domains which were 340 times larger than the initial characteristic eddy size.

The classical pictures of rotating turbulence were reproduced, in which we observed the formation of columnar eddies along the axis of rotation and a decrease in the energy dissipation rate. However, by following the evolution of the integral length scales we identified different dynamics that were shown to depend on Ro_ε . This led us to separate our data-set into 2 groups. While the runs in group *R1* did not show any pronounced sign of growth in the integral length scales, for the runs in group *R2*, ℓ_{\parallel} grew substantially and approximately linearly with time. The latter group of runs can be therefore associated to a regime where the formation of columns predominate, whereas runs of group *R1* are closer to homogeneous isotropic turbulence. Further, we found that the growth rate of the columnar eddies depends exponentially on Ro_ε , i.e., $\gamma = a \exp(b Ro_\varepsilon)$, with $a = 4$ and $b = -17$.

The energy dissipation rate in the group of runs *R1* is well approximated by the scaling law proposed in Baqui & Davidson (2015). For the group *R2*, which consists of runs at lower Ro_ε , we have shown that the scaling laws currently available in the literature fail to approximate ε_ν . Still, we were able to find a similarity relation for ε_ν in the range $0.06 \leq Ro_\varepsilon \leq 0.31$ by applying the ideas introduced by Kraichnan (1965), in which the spectral transfer time is regarded as composed of two opposing time scales. First, by observing the inverse relation between ℓ_{\perp} and ε_ν , we assumed that ℓ_{\perp} was the relevant length scale to form τ_{nl} . Second, the relaxation time scale τ_3 was shown to depend on a power-law of Ro_ε and on τ_{nl}^{iso} , which implies that it is exclusively a function of Ro_ε and of the forcing parameters κ_f and u_f . Thus, we arrived at a similarity law for this Ro_ε range. Scaling ε_ν with $u^4 / (\ell_{\perp}^2 Ro_\varepsilon^{0.62} \tau_{nl}^{iso})$ collapsed the data for different Ro_ε into a single curve.

Last, we would like to remark that the results for the case where the rotation rate is highest, i.e., $Ro_\varepsilon = 0.06$, were verified by increasing the numerical resolution and the domain size by a factor 2 in the direction of rotation. However, whether other dynamics emerge at even lower Ro_ε and the effects of Re_ε remains to be studied. In any case, we hope our numerical investigation provide a useful contribution to the improvement of turbulence models and stimulates other studies to elucidate and quantify the effects of the Coriolis force on the evolution of a cloud of isotropic eddies in unbounded domains.

REFERENCES

- ALVELIUS, K. 1999 Random forcing of three-dimensional homogeneous turbulence. *Physics of Fluids* **11** (7), 1880.
- BAQUI, YASIR BIN & DAVIDSON, P. A. 2015 A phenomenological theory of rotating turbulence. *Physics of Fluids* **27** (2), 025107.
- BARDINA, JORGE, FERZIGER, J. H. & ROGALLO, R. S. 1985 Effect of rotation on isotropic turbulence: computation and modelling. *Journal of Fluid Mechanics* **154** (-1), 321.

- BARTELLO, PETER, MÉTAIS, OLIVIER & LESIEUR, MARCEL 1994 Coherent structures in rotating three-dimensional turbulence. *Journal of Fluid Mechanics* **273** (c), 1–29.
- BATCHELOR, G K & PRESS, CAMBRIDGE UNIVERSITY 1953 *The Theory of Homogeneous Turbulence*. Cambridge University Press.
- BOFFETTA, GUIDO & ECKE, ROBERT E. 2012 Two-Dimensional Turbulence. *Annual Review of Fluid Mechanics* **44** (1), 427–451.
- VAN BOKHOVEN, L. J. A., CLERCX, H. J. H., VAN HEIJST, G. J. F. & TRIELING, R. R. 2009 Experiments on rapidly rotating turbulent flows. *Physics of Fluids* **21** (9), 096601.
- CARDESA, JOSÉ I., VELA-MARTÍN, ALBERTO & JIMÉNEZ, JAVIER 2017 The turbulent cascade in five dimensions. *Science* **357** (6353), 782–784.
- DELACHE, ALEXANDRE, CAMBON, CLAUDE & GODEFERD, FABIEN 2014 Scale by scale anisotropy in freely decaying rotating turbulence. *Physics of Fluids* **26** (2).
- DEUSEBIO, E., BOFFETTA, G., LINDBORG, E. & MUSACCHIO, S. 2014 Dimensional transition in rotating turbulence. *Physical Review E* **90** (2), 023005.
- GALTIER, SÉBASTIEN 2003 Weak inertial-wave turbulence theory. *Physical Review E* **68** (1), 015301.
- GODEFERD, FABIEN S., ED, FR & MOISY, ERIC 2015 Structure and Dynamics of Rotating Turbulence: A Review of Recent Experimental and Numerical Results. *Applied Mechanics Reviews* **67** (3), 030802.
- GREENSPAN, H P 1968 *The Theory of Rotating Fluids*. Cambridge University Press.
- HOPFINGER, E. J., BROWAND, F. K. & GAGNE, Y. 1982 Turbulence and waves in a rotating tank. *Journal of Fluid Mechanics* **125** (-1), 505.
- HUNT, J. C. R., WRAY, A. A. & MOIN, P. 1988 Eddies, streams, and convergence zones in turbulent flows. In *Studying Turbulence Using Numerical Simulation Databases, 2. Proceedings of the 1988 Summer Program*, , vol. 1, pp. 193–208.
- IBBETSON, A. & TRITTON, D. J. 1975 Experiments on turbulence in a rotating fluid. *Journal of Fluid Mechanics* **68**, 639.
- ISHIHARA, TAKASHI, GOTOH, TOSHIYUKI & KANEDA, YUKIO 2009 Study of High Reynolds Number Isotropic Turbulence by Direct Numerical Simulation. *Annual Review of Fluid Mechanics* **41** (1), 165–180.
- JACQUIN, L., LEUCHTER, O., CAMBON, C. & MATHIEU, J. 1990 Homogeneous turbulence in the presence of rotation. *Journal of Fluid Mechanics* **220**, 1–52.
- KANEDA, YUKIO, ISHIHARA, TAKASHI, YOKOKAWA, MITSUO, ITAKURA, KEN'ICHI & UNO, ATSUYA 2003 Energy dissipation rate and energy spectrum in high resolution direct numerical simulations of turbulence in a periodic box. *Physics of Fluids* **15** (2).
- KRAICHNAN, ROBERT H. 1965 Inertial-Range Spectrum of Hydromagnetic Turbulence. *Physics of Fluids* **8** (7), 1385.
- MATTHAEUS, WILLIAM H & ZHOU, YE 1989 Extended inertial range phenomenology of magnetohydrodynamic turbulence. *Physics of Fluids B* **1** (9), 1929–1931.
- MININNI, P. D., ALEXAKIS, A. & POUQUET, A. 2009 Scale interactions and scaling laws in rotating flows at moderate Rossby numbers and large Reynolds numbers. *Physics of Fluids* **21** (1), 015108.
- MININNI, P. D., ROSENBERG, D. & POUQUET, A. 2012 Isotropization at small scales of rotating helically driven turbulence. *Journal of Fluid Mechanics* **699** (1), 263–279.
- MOISY, F., MORIZE, C., RABAUD, M. & SOMMERIA, J. 2011 Decay laws, anisotropy and cyclone-anticyclone asymmetry in decaying rotating turbulence. *Journal of Fluid Mechanics* **666**, 5–35.
- MORINISHI, Y., NAKABAYASHI, K. & REN, S. Q. 2001 New DNS algorithm for rotating homogeneous decaying turbulence. *International Journal of Heat and Fluid Flow* **22** (1), 30–38.
- NAZARENKO, SERGEI V. & SCHEKOCIHIN, ALEXANDER A. 2011 Critical balance in magnetohydrodynamic, rotating and stratified turbulence: towards a universal scaling conjecture. *Journal of Fluid Mechanics* **677**, 134–153, arXiv: 0904.3488.
- PEKUROVSKY, DMITRY 2012 P3DFFT: A Framework for Parallel Computations of Fourier Transforms in Three Dimensions. *SIAM Journal on Scientific Computing* **34** (4), C192–C209.

- PESTANA, TIAGO & HICKEL, STEFAN 2019 Regime transition in the energy cascade of rotating turbulence. *Physical Review E* **99** (5), 053103.
- POPE, S B 2000 *Turbulent Flows*. Cambridge University Press.
- ROGALLO, R. S. 1977 An ILLIAC program for the numerical simulation of homogeneous incompressible turbulence. *NASA Technical Memo* **73**, 203.
- SESHASAYANAN, KANNABIRAN & ALEXAKIS, ALEXANDROS 2018 Condensates in rotating turbulent flows. *Journal of Fluid Mechanics* **841**, 434–462.
- SMITH, LESLIE M., CHASNOV, JEFFREY R. & WALEFFE, FABIAN 1996 Crossover from Two- to Three-Dimensional Turbulence. *Physical Review Letters* **77** (12), 2467–2470.
- STAPLEHURST, P J, DAVIDSON, P A & DALZIEL, S B 2008 Structure formation in homogeneous freely decaying rotating turbulence. *Journal of Fluid Mechanics* **598**, 81–105.
- TANG, S. L., ANTONIA, R. A., DJENIDI, L., DANAILA, L. & ZHOU, Y. 2018 Reappraisal of the velocity derivative flatness factor in various turbulent flows. *Journal of Fluid Mechanics* **847**, 244–265.
- VALENTE, PEDRO C. & DALLAS, VASSILIOS 2016 Spectral imbalance in the inertial range dynamics of decaying rotating turbulence **023114**, 1–8, arXiv: 1610.05032.
- VAN ATTA, C. W. & ANTONIA, R. A. 1980 Reynolds number dependence of skewness and flatness factors of turbulent velocity derivatives. *Physics of Fluids* **23** (2), 252–257.
- YEUNG, P. K. & ZHOU, YE 1998 Numerical study of rotating turbulence with external forcing. *Physics of Fluids* **10** (11), 2895.
- YOSHIMATSU, K., MIDORIKAWA, M. & KANEDA, Y. 2011 Columnar eddy formation in freely decaying homogeneous rotating turbulence. *Journal of Fluid Mechanics* **677**, 154–178.
- ZEMAN, O. 1994 A note on the spectra and decay of rotating homogeneous turbulence. *Physics of Fluids* **6** (10), 3221.
- ZHOU, YE 1995 A phenomenological treatment of rotating turbulence. *Physics of Fluids* **7** (8), 2092.